



Global El Niño–Southern Oscillation Teleconnections in CMIP6 Models

Ilya V. Serykh * and Dmitry M. Sonechkin †

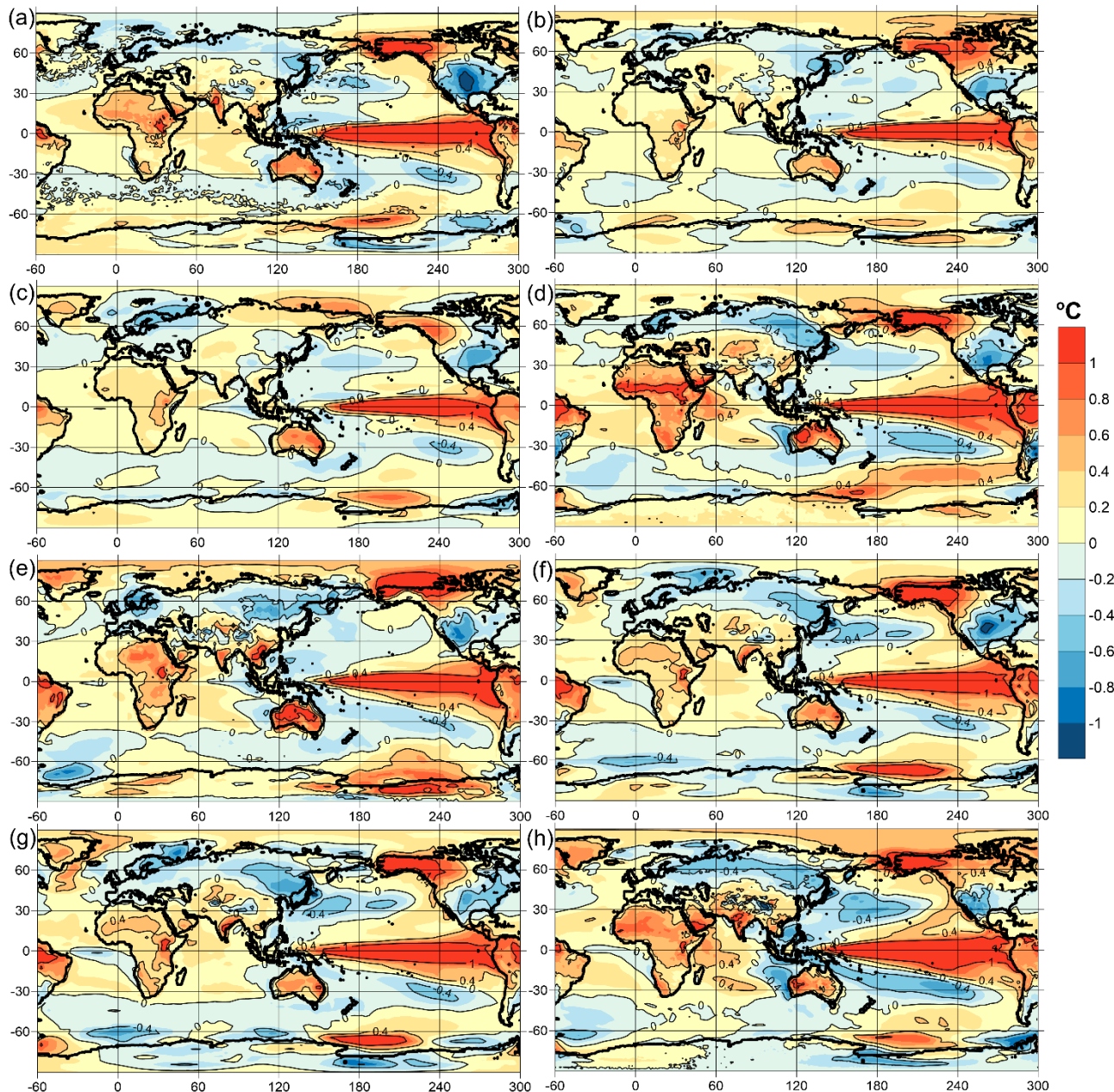


Figure S1. Difference fields of average surface temperature anomalies between opposite phases of ENSO according to ONI for models: AWI AWI-CM-1-1-MR (a), BCC BCC-CSM2-MR (b), BCC BCC-ESM1 (c), CAS CAS-ESM2-0 (d), CAS FGOALS-g3 (e), CCCma CanESM5 (f), CCCma CanESM5-CanOE (g), CMCC CMCC-CM2-SR5 (h).

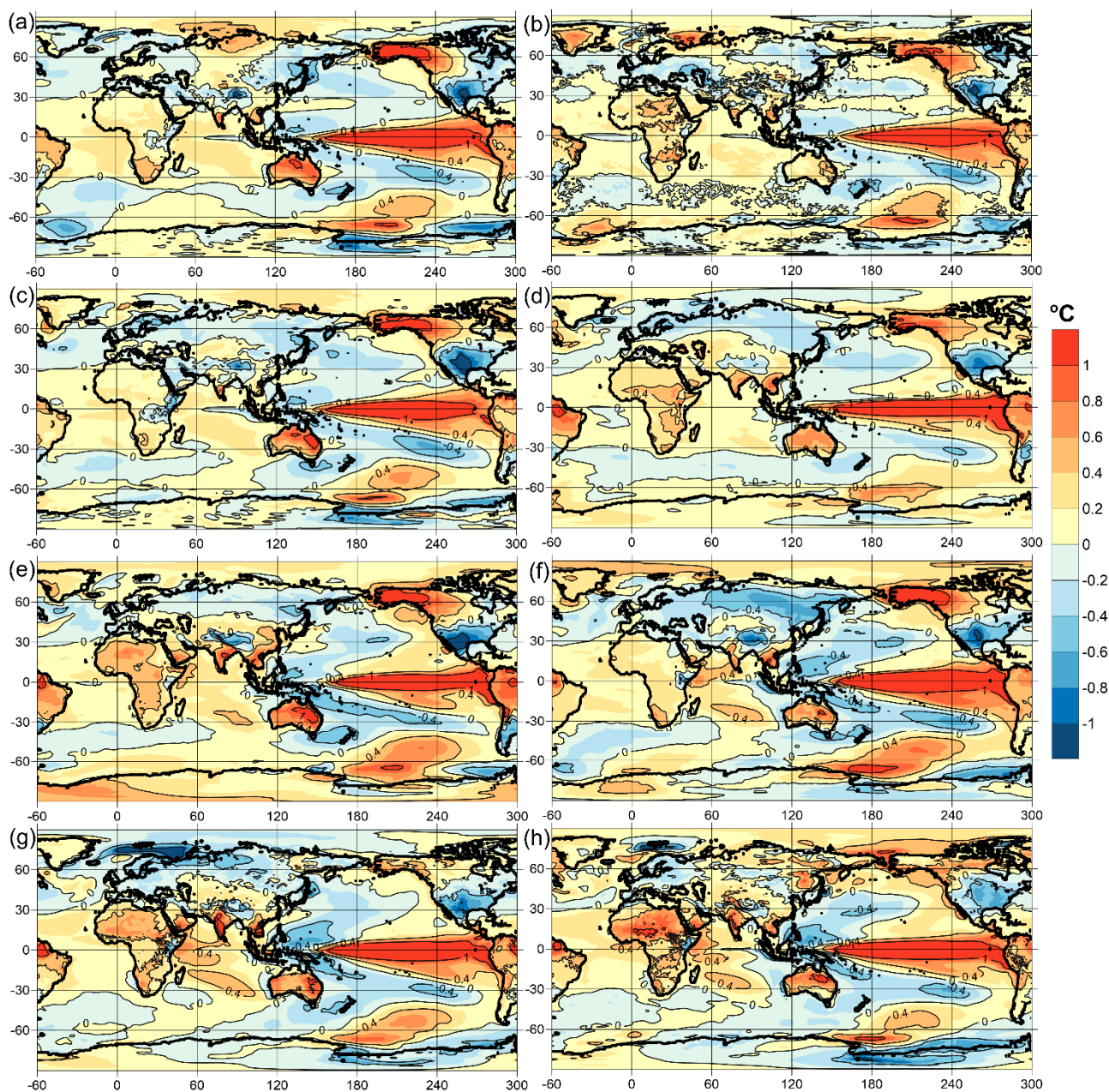


Figure S2. Difference fields of average surface temperature anomalies between opposite phases of ENSO according to ONI for models: CNRM-CERFACS CNRM-CM6-1 (a), CNRM-CERFACS CNRM-CM6-1-HR (b), CNRM-CERFACS CNRM-ESM2-1 (c), CSIRO ACCESS-ESM1-5 (d), CSIRO-ARCCSS ACCESS-CM2 (e), E3SM-Project E3SM-1-0 (f), EC-Earth-Consortium EC-Earth3 (g), EC-Earth-Consortium EC-Earth3-AerChem (h).

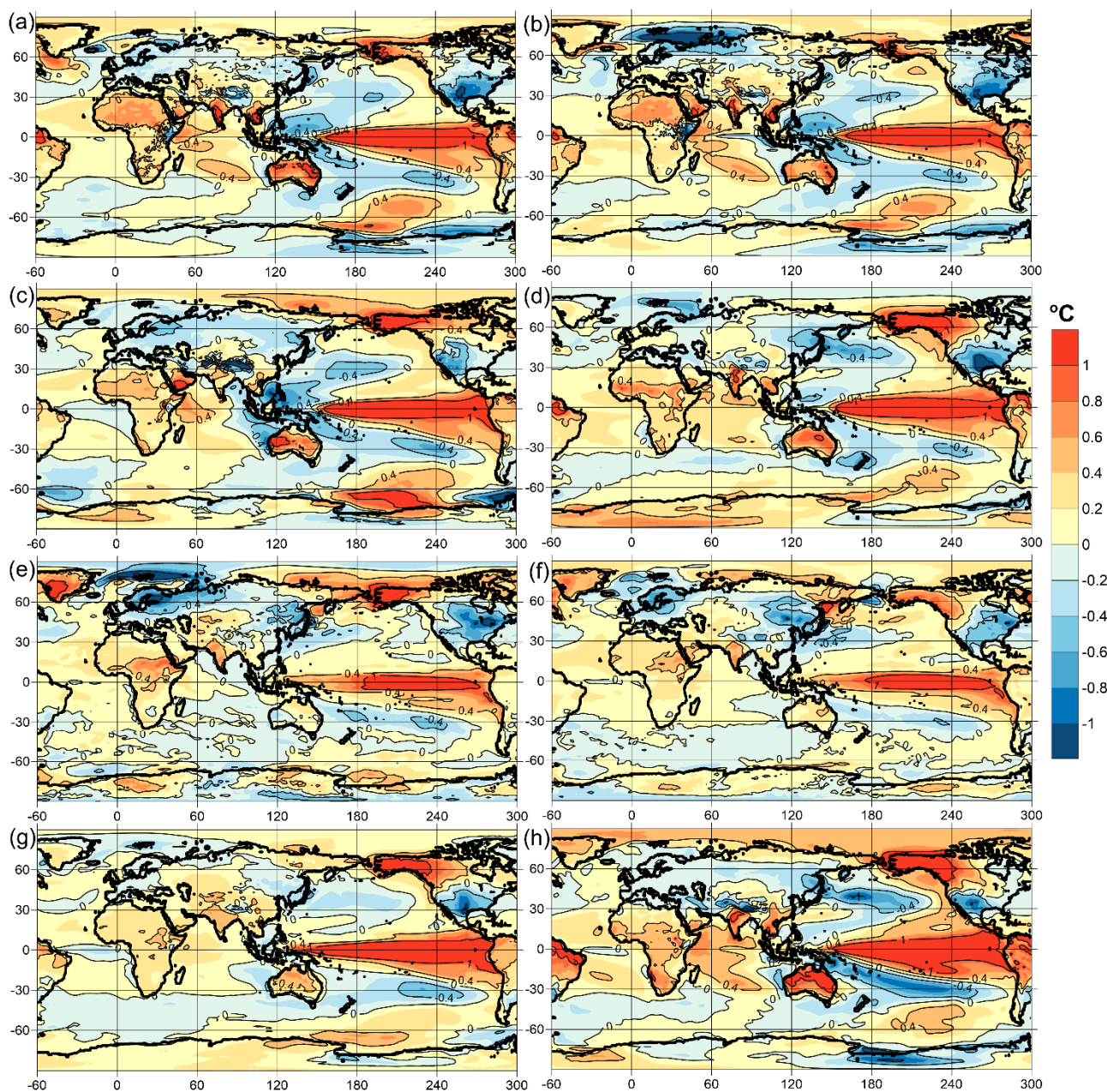


Figure S3. Difference fields of average surface temperature anomalies between opposite phases of ENSO according to ONI for models: EC-Earth-Consortium EC-Earth3-Veg (a), EC-Earth-Consortium EC-Earth3-Veg-LR (b), FIO-QLNM FIO-ESM-2-0 (c), HAMMOZ-Consortium MPI-ESM-1-2-HAM (d), INM INM-CM4-8 (e), INM INM-CM5-0 (f), IPSL IPSL-CM6A-LR (g), MIROC MIROC6 (h).

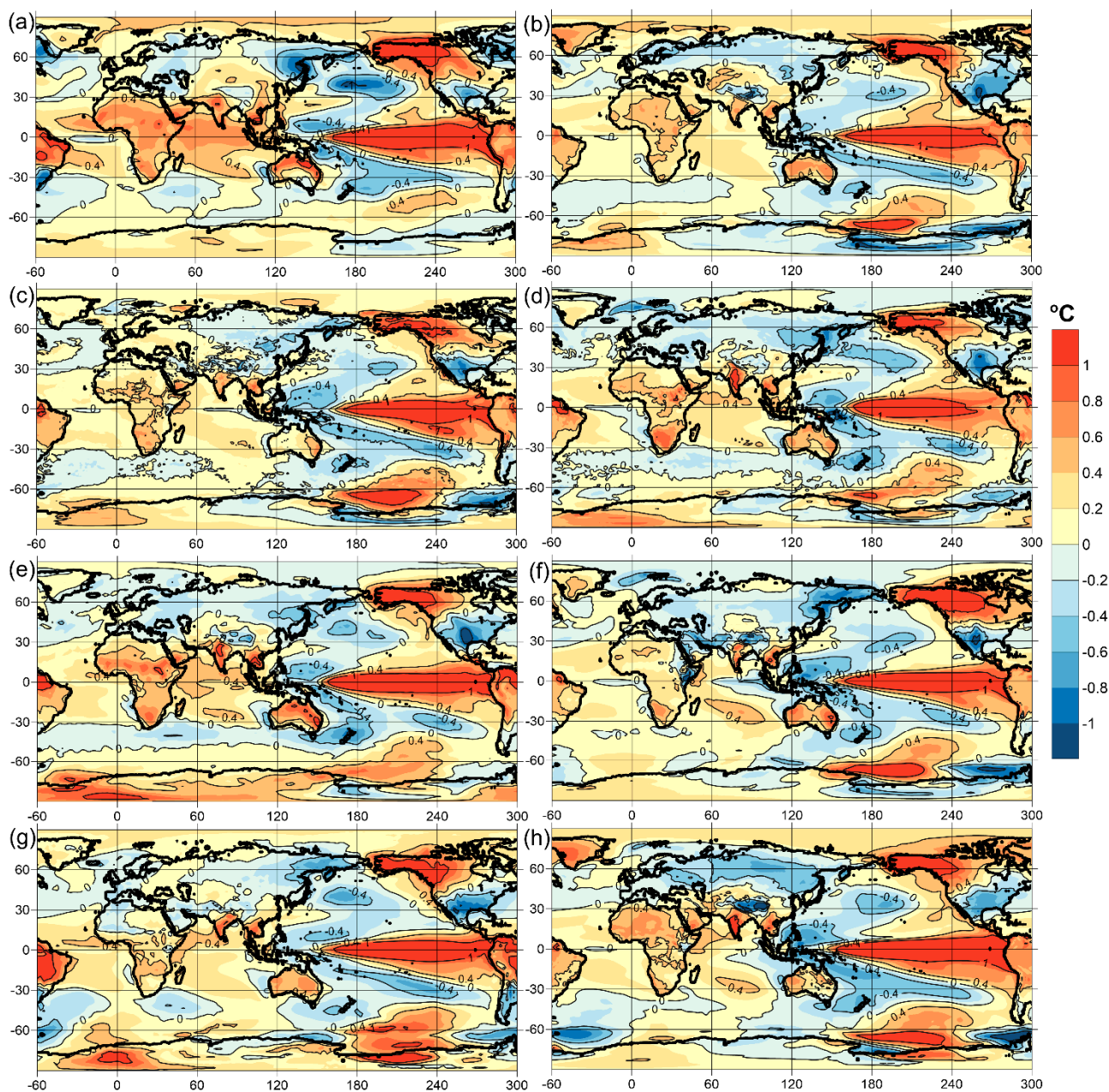


Figure S4. Difference fields of average surface temperature anomalies between opposite phases of ENSO according to ONI for models: MIROC MIROC-ES2L (a), MOHC HadGEM3-GC31-LL (b), MOHC HadGEM3-GC31-MM (c), MPI-M MPI-ESM1-2-HR (d), MPI-M MPI-ESM1-2-LR (e), MRI MRI-ESM2-0 (f), NASA-GISS GISS-E2-1-H (g), NCAR CESM2 (h).

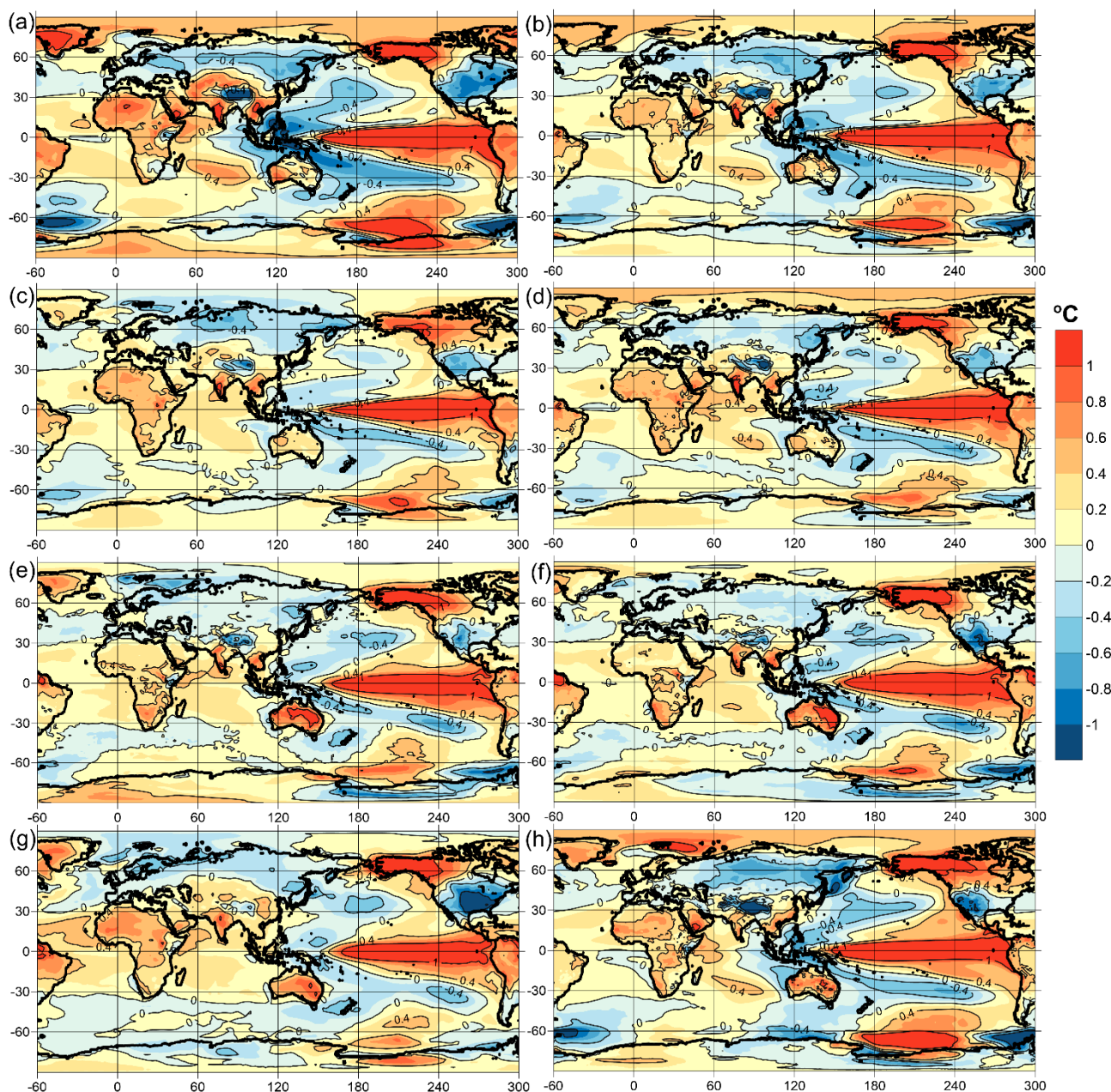


Figure S5. Difference fields of average surface temperature anomalies between opposite phases of ENSO according to ONI for models: NCAR CESM2-FV2 (a), NCAR CESM2-WACCM (b), NCC NorESM2-LM (c), NCC NorESM2-MM (d), NOAA-GFDL GFDL-CM4 (e), NOAA-GFDL GFDL-ESM4 (f), NUIST NESM3 (g), SNU SAM0-UNICON (h).

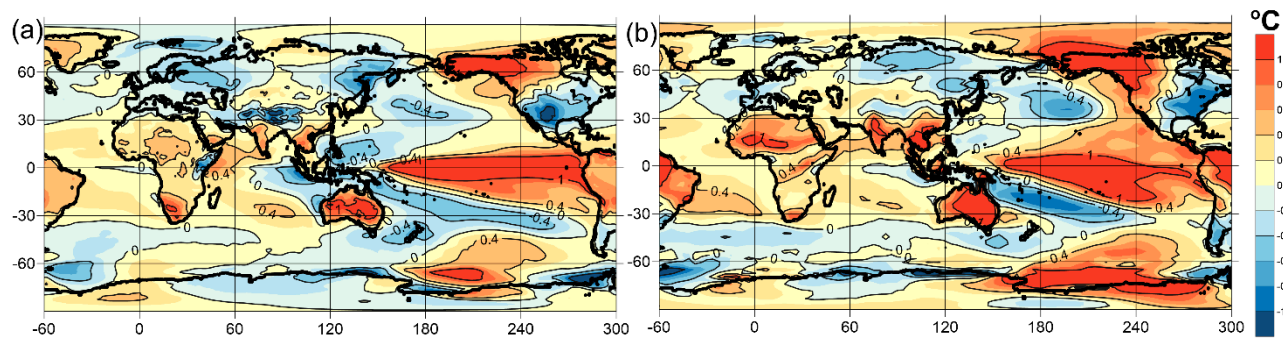


Figure S6. Difference fields of average surface temperature anomalies between opposite phases of ENSO according to ONI for models: THU CIESM (a), UA MCM-UA-1-0 (b).

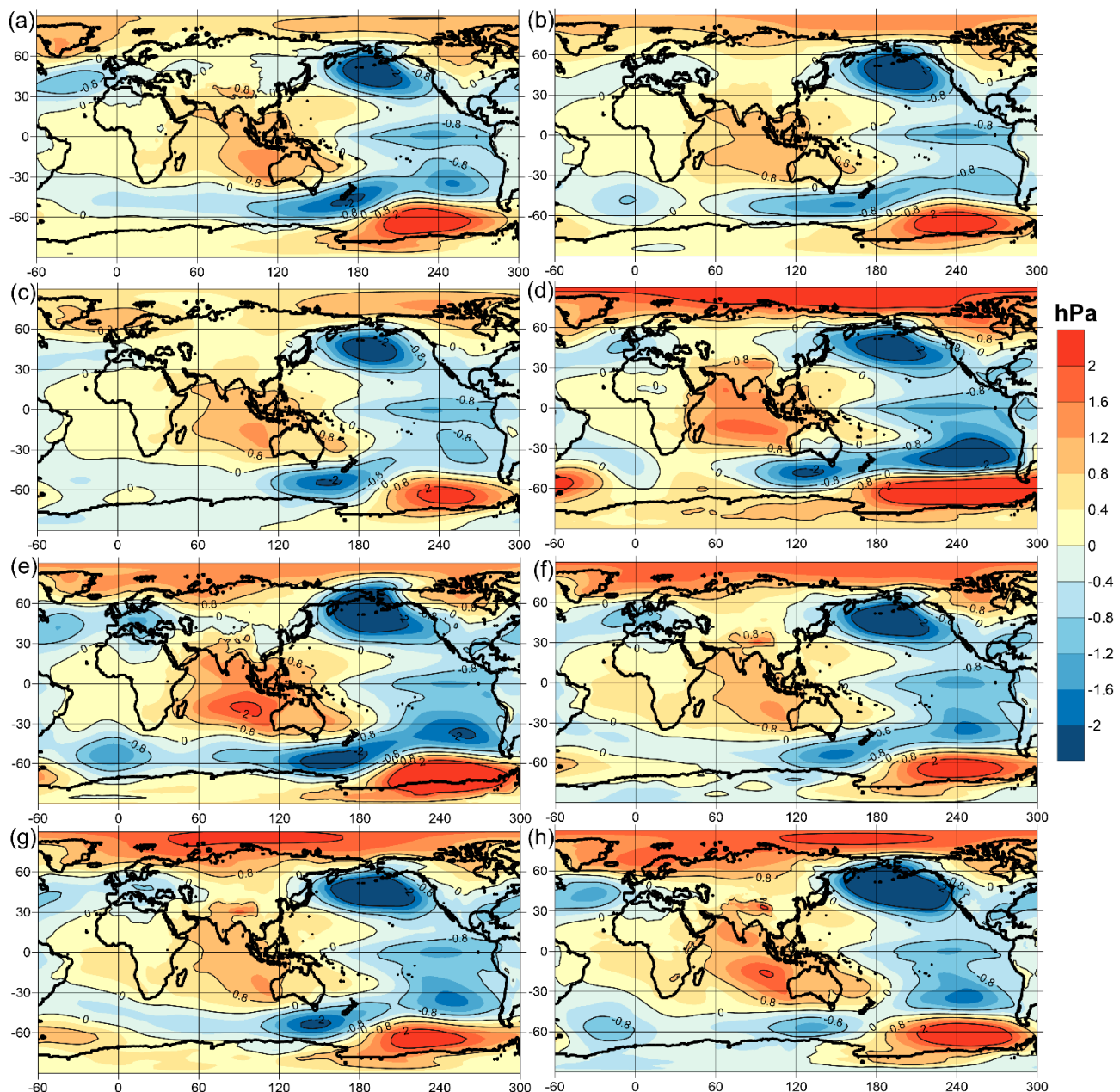


Figure S7. Difference fields of average sea level pressure anomalies between opposite phases of ENSO according to ONI for models: AWI AWI-CM-1-1-MR (a), BCC BCC-CSM2-MR (b), BCC BCC-ESM1 (c), CAS CAS-ESM2-0 (d), CAS FGOALS-g3 (e), CCCma CanESM5 (f), CCCma CanESM5-CanOE (g), CMCC CMCC-CM2-SR5 (h).

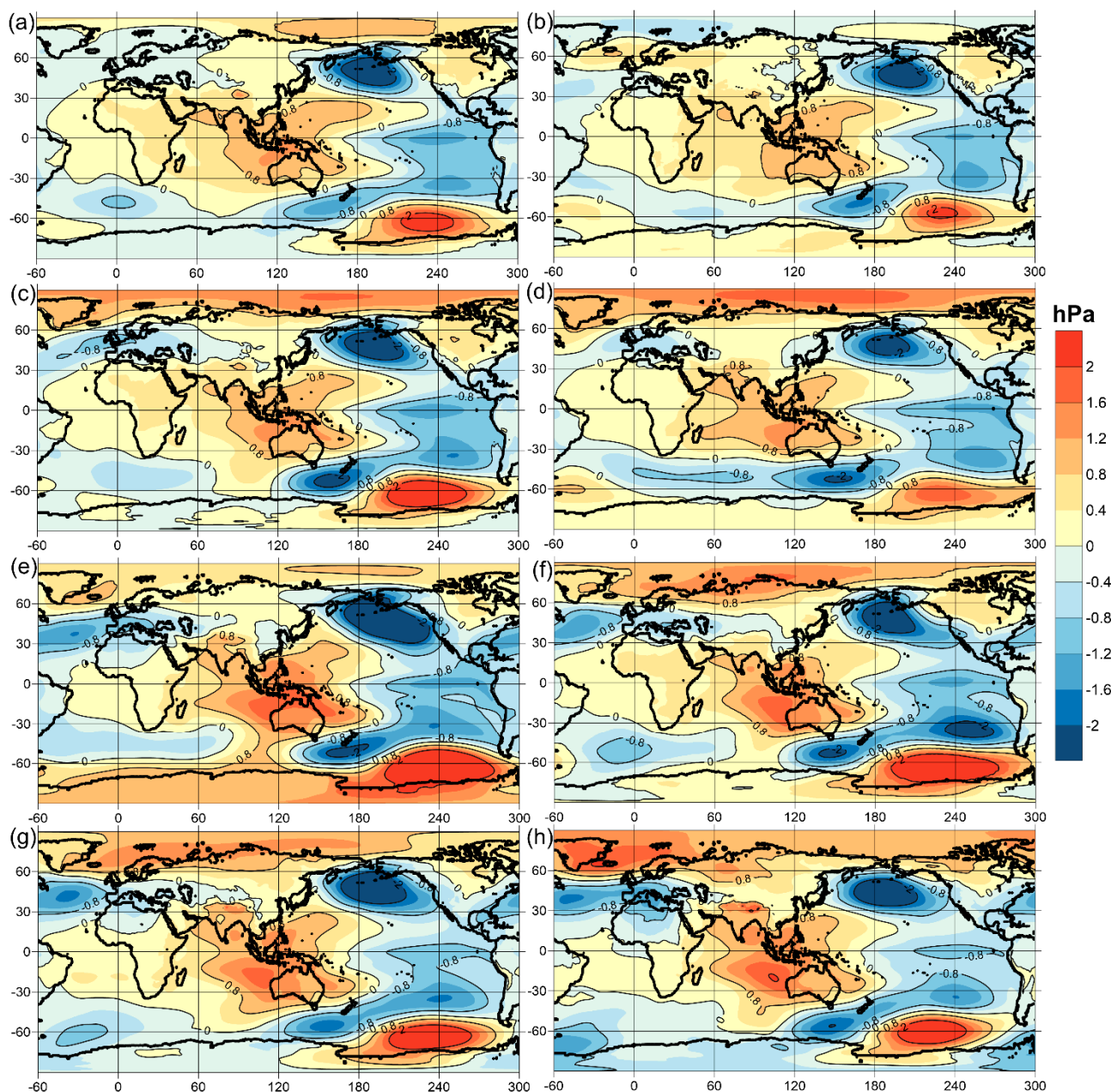


Figure S8. Difference fields of average sea level pressure anomalies between opposite phases of ENSO according to ONI for models: CNRM-CERFACS CNRM-CM6-1 (a), CNRM-CERFACS CNRM-CM6-1-HR (b), CNRM-CERFACS CNRM-ESM2-1 (c), CSIRO ACCESS-ESM1-5 (d), CSIRO-ARCCSS ACCESS-CM2 (e), E3SM-Project E3SM-1-0 (f), EC-Earth-Consortium EC-Earth3 (g), EC-Earth-Consortium EC-Earth3-AerChem (h).

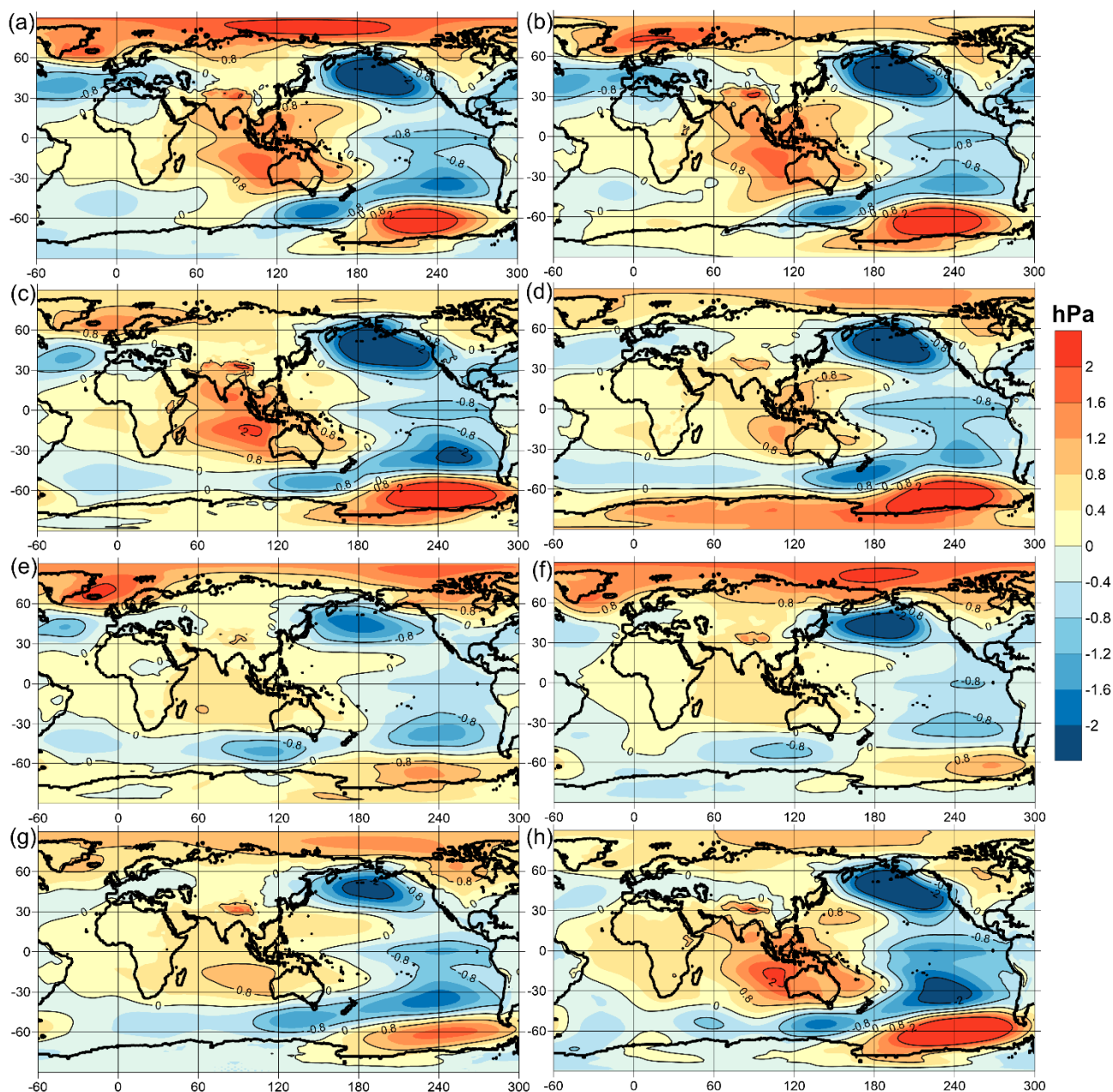


Figure S9. Difference fields of average sea level pressure anomalies between opposite phases of ENSO according to ONI for models: EC-Earth-Consortium EC-Earth3-Veg (a), EC-Earth-Consortium EC-Earth3-Veg-LR (b), FIO-QLNM FIO-ESM-2-0 (c), HAMMOZ-Consortium MPI-ESM-1-2-HAM (d), INM INM-CM4-8 (e), INM INM-CM5-0 (f), IPSL IPSL-CM6A-LR (g), MIROC MIROC6 (h).

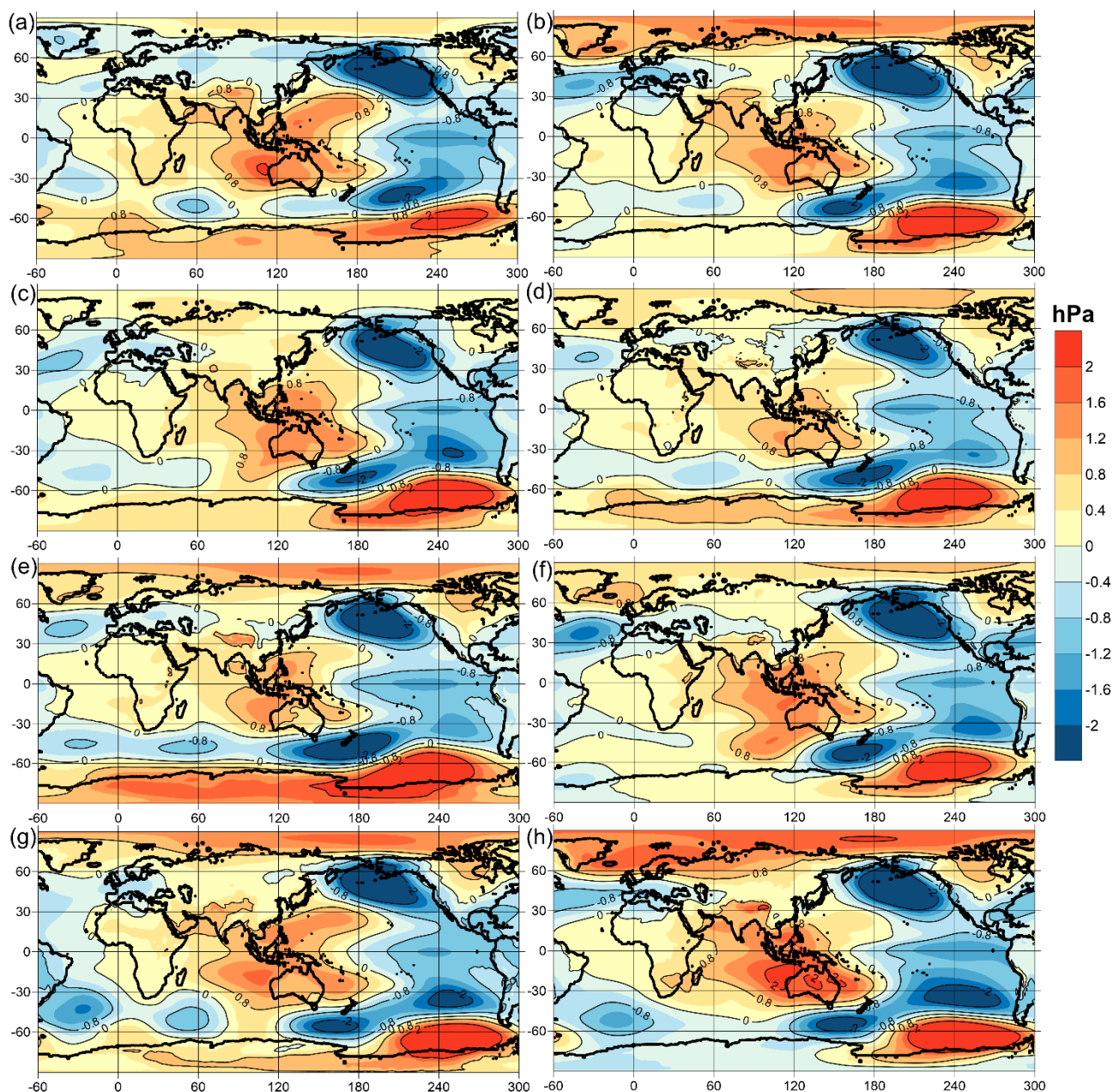


Figure S10. Difference fields of average sea level pressure anomalies between opposite phases of ENSO according to ONI for models: MIROC MIROC-ES2L (a), MOHC HadGEM3-GC31-LL (b), MOHC HadGEM3-GC31-MM (c), MPI-M MPI-ESM1-2-HR (d), MPI-M MPI-ESM1-2-LR (e), MRI MRI-ESM2-0 (f), NASA-GISS GISS-E2-1-H (g), NCAR CESM2 (h).

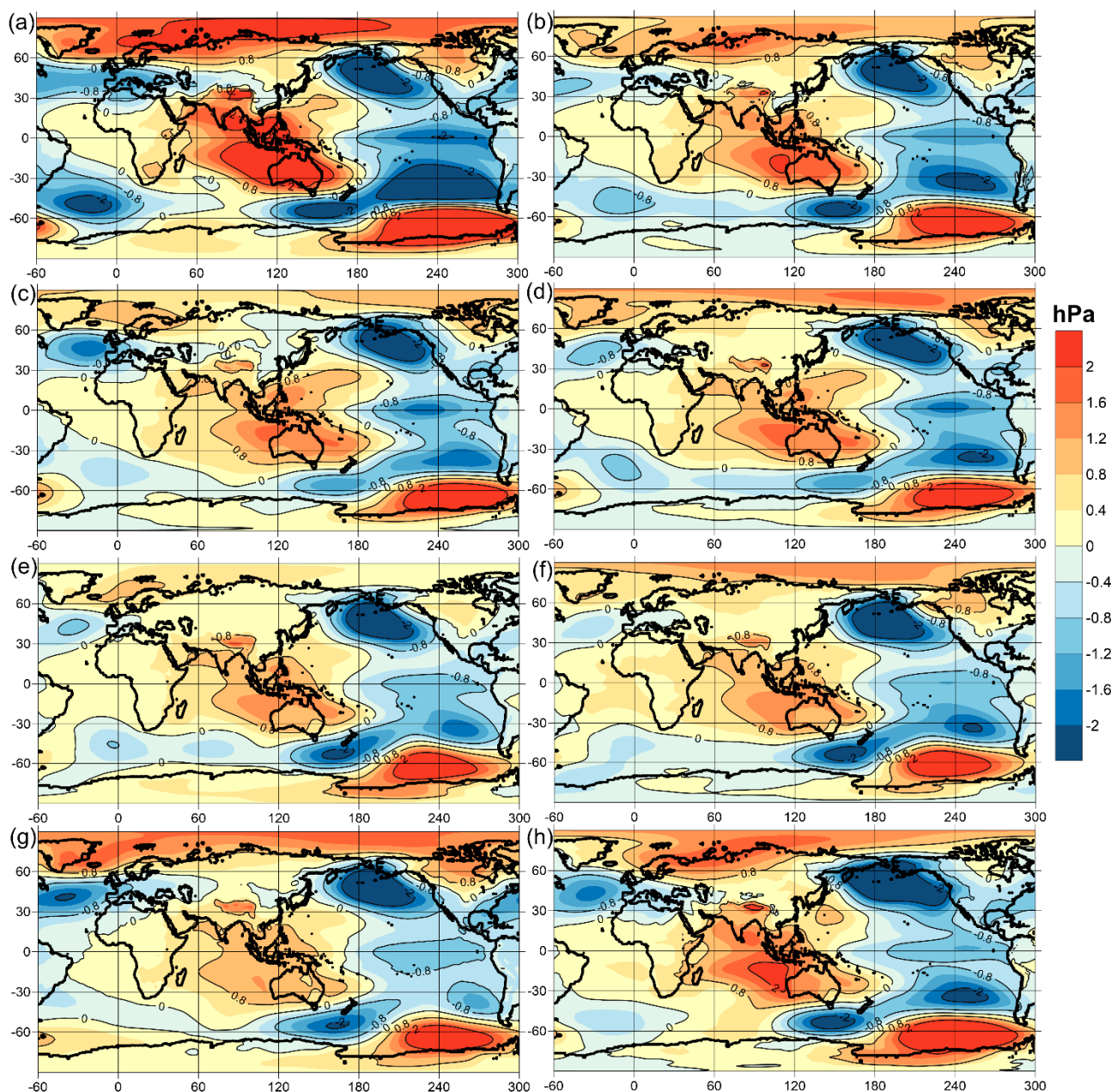


Figure S11. Difference fields of average sea level pressure anomalies between opposite phases of ENSO according to ONI for models: NCAR CESM2-FV2 (a), NCAR CESM2-WACCM (b), NCC NorESM2-LM (c), NCC NorESM2-MM (d), NOAA-GFDL GFDL-CM4 (e), NOAA-GFDL GFDL-ESM4 (f), NUIST NESM3 (g), SNU SAM0-UNICON (h).

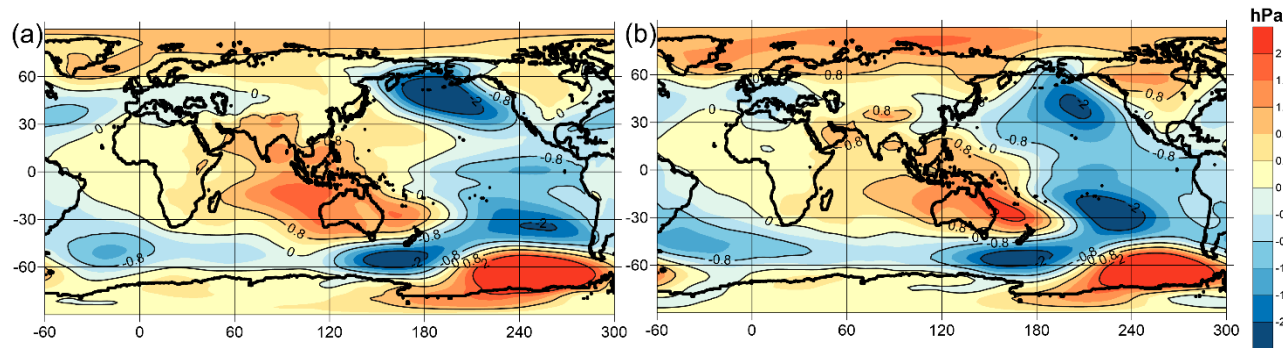


Figure S12. Difference fields of average sea level pressure anomalies between opposite phases of ENSO according to ONI for models: THU CIESM (a), UA MCM-UA-1-0 (b).